How Narrow is the Linewidth of Parametric X-Ray Radiation?

K.-H. Brenzinger, B. Limburg, H. Backe, S. Dambach, H. Euteneuer, F. Hagenbuck, C. Herberg, K. H. Kaiser, O. Kettig, G. Kube, W. Lauth, H. Schöpe, and Th. Walcher

Institut für Kernphysik, Fachbereich Physik, Johannes Gutenberg Universität, D-55099 Mainz, Germany

(Received 21 February 1997)

Parametric x-ray or quasi-Cherenkov radiation is produced by the passage of an electron through a crystal. A critical absorber technique has been employed to investigate its linewidth. Experiments have been performed with the 855 MeV electron beam from the Mainz Microtron MAMI. Thin absorber foils were mounted in front of a CCD camera serving as a position sensitive photon detector. Upper limits of the linewidth of 1.2 and 3.5 eV were determined for the (111) and (022) reflections of silicon at photon energies of 4966 and 8332 eV. These limits originate from geometrical line broadening effects that can be optimized to reach the ultimate limit given by the finite length of the wave train. [S0031-9007(97)04050-7]

PACS numbers: 61.10.–i, 41.50.+h, 41.60.–m, 78.70.Dm

Parametric x-ray radiation (PXR) is produced when charged particles traverse a crystal. This radiation can be understood as the coherent superposition of the elementary waves emitted from the atoms which are induced by the electromagnetic field of the passing particle. In an equivalent picture they can be described as the diffraction of the virtual photons associated with the moving particles or as a quasi-Cherenkov radiation in a medium with a periodic dielectricity. The most intriguing feature of PXR is the appearance of a sharp quasimonochromatic x-ray beam close to the Bragg angle. The narrow angular distribution consists of one peak above and one below the symmetry plane of the crystal. Their widths are characterized by the angle $\theta_{\mathrm{ph}} = [1/\gamma^2 + (\omega_p/\omega)^2]^{1/2}$, with γ the Lorentz factor of the moving particle, ω the angular frequency of the emitted photon, and ω_p the plasma frequency of the crystal, 31 eV for Si. The theoretical description of the intensity distribution of PXR [1–5], suitably modified for self-absorption and multiple scattering effects, have been tested in a broad range of electron energies extending from 3.5 MeV [6,7] to about 1 GeV [8]. It was found to be accurate within 12%. On the other hand, very little is known about the energy width of PXR. The various theoretical descriptions of PXR predict a very narrow linewidth of less than a few meV. Actually, if it is assumed that a charged particle passes a very thick and perfect single crystal on a straight line and if self-absorption of the photons in the crystal can be neglected, simply a δ function results for the line shape. Measurements of the linewidth have been performed up to now at the low beam energy of 6.8 MeV only. A variance of the linewidth of 48 eV has been determined for a 55 μm thick diamond crystal at a photon energy of 8.98 keV [9]. This rather large linewidth originates at low electron energy from the multiple scattering of electrons in the crystal.

In this Letter a measurement of PXR at the Mainz Microtron MAMI with a silicon crystal at photon energies of about 5.0 and 8.3 keV is presented. For the high beam energy of MAMI of 855 MeV a line broadening by multiple scattering of the electrons in the crystal can be neglected. This fact originates from the rather surprising result that the angular beam spread enters as a second order effect into the energy width of PXR (see below). A very important consequence of this new insight is that with low emittance high energy beams from modern electron accelerators the natural linewidth of PXR should be reachable. This width is predicted to be significantly narrower as the Darwin width of low order Bragg reflexes from perfect crystals. Beyond the insight in the PXR mechanism these investigations show that a quasimonochromatic photon beam can be prepared in a rather simple way. Such a photon beam excels by a narrow bandwidth without a monochromator, easy tunability, low background due to a large emission angle, and most importantly a possibility to trigger with a resolution of down to a few ps. Applications of PXR using some of these features are discussed in Ref. [1,10–12].

The line broadening contributions can be subdivided into a natural, a geometrical, and an intrinsic one. The natural linewidth of PXR results from the photon self-absorption which brings about an exponentially increasing wave train terminating abruptly if the electron leaves the crystal. The Fourier transform of this wave train has a Lorentzian shape with a width $\Gamma = \hbar/\tau_{\mathrm{eff}}$ determined by the effective "photon lifetime" τ_{eff} [13]. The geometrical contribution to the linewidth originates (i) from the spread $\Delta\theta_D$ of the observation angle θ_D caused by the beam spot size x and the position resolution w of the detector, (ii) from the angular spread $\Delta\alpha_x$ of the electron beam, and (iii) from the angular spread $\Delta\theta_{\mathrm{sc}}$ by scattering of the electrons in the crystal. An intrinsic linewidth may originate from crystal imperfections as there are possibly mosaic structure displacements, or even mechanical distortions of the crystal. If they are present a broadening will be caused either by the directional variance of the reciprocal lattice vector or by random phase changes in the emitted wave train.

 0031-9007/97/79(13)/2462(4)$10.00

The following discussion of these line broadening effects will be carried out on the basis of the general expression for the photon energy [1]

$$\hbar\omega = \hbar c \frac{|\hat{n}\vec{\tau}|}{1/\beta - \sqrt{\varepsilon_0}\,\hat{n}\hat{k}}, \tag{1}$$

with $\hat{n}$ the direction of the electron with velocity vector $\vec{v}$, $\vec{\tau}$ the reciprocal lattice vector with $\tau = 2\pi/d_{hkl}$, $d_{hkl} = d/(h^2 + k^2 + l^2)^{1/2}$ the spacing between the lattice planes and h, k, l the Miller indices, $\vec{k}$ the wave vector of the emitted photon, and ε_0 the mean dielectric constant. The photon wave vector $\vec{k}$ is assumed to lie in the plane spanned by $\hat{n}$ and $\vec{\tau}$. As usual $\beta = v/c$ and ε_0 can be approximated by 1. These restrictions and approximations are well justified at high beam energies and at photon energies $\geq$5 keV. The deviation of an individual electron from the beam direction is described in this plane by the angle α_x, x being the horizontal coordinate in Fig. 1 in the plane spanned by $\hat{n}$ and $\vec{\tau}$. The observation angle θ_D must be close to twice the Bragg angle θ_B so that the deviation $\theta_x = 2\theta_B - \theta_D$ is in the order of the characteristic angle $\theta_{\rm ph}$. Under these conditions the photon energy can be approximated as

$$\hbar\omega = \hbar c\tau \frac{\sin(\theta_B + \alpha_x)}{2\sin^2[(\theta_D + \alpha_x)/2]}, \tag{2}$$

which coincides with Bragg's law if $\alpha_x = 0$ and $\theta_D = 2\theta_B$. From Eq. (2) and the schematic drawing of the experimental setup in Fig. 1 the basic idea of the critical absorber technique can be understood. The PXR-intensity distribution shows in θ_y direction two peaks above and below the horizontal plane (see, e.g., Ref. [8]). In θ_x direction for each $\hbar\omega$ a peak with the line width of Γ is superimposed to give the total distribution. The energy width of the total distribution is cut by a slit defining $\Delta\theta_x$. If one brings an absorber foil with a suitable K-edge energy in the PXR intensity the superposition of PXR lines is convoluted with the narrow K edge having a typical width of a few eV. This convoluted intensity distribution is measured with a CCD camera [pixel size 22 μm, sensitivity depth (44 $\pm$ 20) μm]. It is positioned at an angle $2\theta_B$ of about 45° with respect to the electron beam direction at a distance of $L = 1010$ mm. First results of this investigation were communicated in Ref. [14].

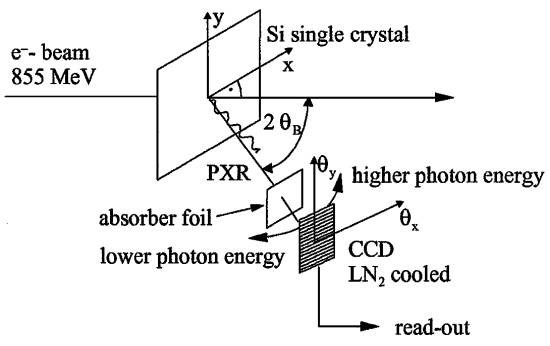

FIG. 1. Schema of the experimental setup for the measurement of the linewidth using a critical absorber technique. The silicon crystal has a thickness $t = 124$ μm and is cut with the (100) plane parallel to the surface.

For the measurement of the (111) reflection corresponding to $\hbar\omega = 4966$ eV the crystal has been tilted counterclockwise by an angle $\theta_t = 12°$ and for the measurement at the (022) plane corresponding to $\hbar\omega = 8332$ eV clockwise by $\theta_t = -23°$ around the vertical axis. This special geometry requires the introduction of a factor $a = \cos(\theta_D + \theta_t)/\cos\theta_t$ with $a = 0.557$ and 1.0 for $\hbar\omega = 4966$ and 8332 eV, respectively.

The natural linewidth is given by $\Gamma = \hbar c/(aL_a)$ with the effective photon lifetime $\tau_{\rm eff} = aL_a/c$. Here aL_a is the effective absorption length as measured in the direction of the electron velocity vector. With the photon absorption length $L_a = 17.5$ μm for $\hbar\omega = 4966$ eV a $\Gamma = 20$ meV results and with $L_a = 78$ μm for $\hbar\omega = 8332$ eV a $\Gamma = 2.5$ meV.

Beam spot size, electron path length, and detector aperture determine a geometrical photon energy spread $\Delta\hbar\omega/\hbar\omega|_{\alpha_x=0} = -\Delta\theta_D/\tan(\theta_D/2)$ at a constant angle $\alpha_x = 0$ where the rms angle $\Delta\theta_D = \{(ax)^2 + (1/12) \times \{L_a a \sin\theta_D/[1 + (L_a/d)a\cos\theta_t]\}^2 + (1/12)(w)^2\}^{1/2}/L$. The angular spread $\Delta\alpha_x$ of the electron beam produces a contribution $\Delta\hbar\omega/\hbar\omega|_{\theta_D=\rm const} = [-2 \cdot \theta_x \cdot \Delta\alpha_x - (\Delta\alpha_x)^2]/[4\sin^2(\theta_D/2)]$. It is worth noticing that this line broadening is second order in $\Delta\alpha_x$ and therefore small if an observation angle θ_D close to $2\theta_B$ is chosen, i.e., if $|\theta_x| \ll \Delta\alpha_x/2$. Since the beam spot size enters linearly in the energy width, an optimal focusing can be achieved with a small spot size but a rather large beam divergence. Both geometrical contributions have to be added quadratically. Minimization of the resulting $\Delta\hbar\omega/\hbar\omega$ after substitution of $\Delta\alpha_x$ through the electron beam emittance $\epsilon_x = \pi\,\Delta\alpha_x\,\Delta x$ yields for the relative rms width

$$\left.\frac{\Delta\hbar\omega}{\hbar\omega}\right|_{\rm opt}^{\rm geo} \cong \left[(2^{-2/3} + 2^{1/3})\left(\frac{\epsilon_x a\cos(\theta_D/2)}{2\pi L\sin^2(\theta_D/2)}\right)^{4/3} + \frac{1}{12}\left(\frac{(L_a/L)a\sin\theta_D}{[1 + (L_a/d)a\cos\theta_t]\tan(\theta_D/2)}\right)^2 + \frac{1}{12}\left(\frac{w}{L\tan(\theta_D/2)}\right)^2\right]^{1/2}, \tag{3}$$

with an optimal beam spot size

$$x_{\rm opt} = 2^{1/6}\left(\frac{\epsilon_x}{2\pi\sin\theta_B}\right)^{2/3}\left(\frac{L}{a}\tan\theta_B\right)^{1/3}. \tag{4}$$

The three terms in Eq. (3) result from beam emittance, length of the visible electron path, and the spatial resolution of the detector, respectively. With a horizontal beam emittance $\epsilon_x = 7\pi$ nm rad (1σ) of MAMI at 855 MeV and the parameters quoted above a $\Delta\hbar\omega|_{\rm opt}^{\rm geo} = 0.09$ eV (1σ) and $\Delta\hbar\omega|_{\rm opt}^{\rm geo} = 0.3$ eV (1σ) result for $\hbar\omega = 4966$ eV and

$\hbar\omega = 8332$ eV, respectively. The optimal beam spot size is $x_{\text{opt}} \simeq 4\ \mu$m ($1\sigma$). In comparison with these numbers the broadening caused by multiple scattering is more than a factor of 40 less, justifying its neglect in Eq. (3).

The possible contribution of the intrinsic linewidth can, in principle, be obtained by unfolding from the total linewidth the geometrical contribution. For this the very small spot size of the electron beam must be measured with very high accuracy which is practically difficult. Therefore, the measurement will yield an upper limit for the intrinsic linewidth only.

Because of the dominating geometrical effects the usage of a crystal spectrometer is not adequate. A much better alternative is offered by using the steep K-absorption edge of suitable elements for which the absorption coefficient changes by about 1 order of magnitude within a few eV [14]. If such an absorber foil is brought in front of the CCD detector the transmitted PXR intensity reflects the K-absorption edge structures convoluted with the PXR linewidth. The energy can be obtained via Eq. (2) from the emission angles θ_D of the photons as determined with the spatially resolving CCD detector.

In the experiment an 8 μm thick titanium and a 6 μm thick nickel foil have been used with the K-absorption edges at 4966 and 8332 eV, respectively. Of course, for a high resolution measurement in the order of 1 eV the x-ray absorption near edge fine structure (XANES) has to be taken into account. Measurements of the linear attenuation coefficients $\mu(\hbar\omega)$ performed at synchrotron radiation sources with a typical resolution of 1 eV [15,16] have been used. The derivatives of the transmission functions exhibit structures with widths of 1.6 and 2.9 eV (FWHM) for Ti and Ni, respectively.

The experimental setup is almost the same as for a previous measurement in which the angular distribution of PXR was investigated [8]. The only change is the use of a CCD chip, as described above, as an x-ray detector. The CCD is cooled with LN_2 to reduce the readout noise. It is operated in a single-event mode which means that each single photon event is read out.

The continuous-wave electron beam of MAMI was focused on the silicon crystal with a spot size of (75 ± 25) μm (1σ). This spot size is by a factor of 20 larger as the optimum one of about 4 μm (1σ) and results in estimated geometrical linewidths of 1.2 eV (FWHM) and 3.6 eV (FWHM) for the photon energies of 4966 and 8332 eV, respectively. These geometrical linewidths are about the same as the widths of the XANES structures in the derivatives of the transmission functions for Ti and Ni.

To avoid double counting of photons within one CCD pixel the electron beam was limited to several nA and the exposure time was 0.25 s per image. In a first experimental step the PXR distributions without absorber material were recorded. In a second step the measurements were repeated with the absorbing foils moved into the photon beam. In order to extract images and reduce the background noise the following procedure has been applied to the raw data. First a pulse high spectrum has been produced by accumulating the events from each single data. Only those photons were selected whose energy was in an interval of ± 450 eV around the center of the selected PXR peak. The energy resolution of the detector is (225 ± 11) eV (1σ). The coordinates of all photon events within the energy cuts are finally collected in a scatter plot as shown in Fig. 2. These are the first energy resolved spatial PXR images ever measured. The intensity distribution represents a direct image of the two-dimensional angular distribution of parametric x-ray radiation (see also Fig. 1 of Ref. [8]). It can be seen from the intensity close to the symmetry line that fingerprints of transition diffracted radiation (TDR), i.e., a circle with maximum at $\theta_{\text{TDR}}^{\max} = 1/\gamma = 0.6$ mrad, are absent (for orientation: the PXR maxima are located at $\theta_{\text{PXR}}^{\max} = (\omega_p/\omega) = \pm 3.7$ mrad). The effect of the absorption edges of the absorber material is clearly visible. The left side of the image corresponds to high energy photons for which the absorption coefficient of the photons is high.

The transmitted intensity $T(\hbar\omega)$ has been obtained by projecting the sum images along the nondispersive θ_y axis and transforming the angle θ_x in the photon energy according to Eq. (2). The result for titanium is shown in Fig. 3.

The transmitted intensity $T(\hbar\omega)$ has been fitted by the expression

$$T_{\text{fit}}(\hbar\omega(\theta_x)) = N \int [T_{\mu a}(\hbar\omega') \otimes g(\hbar\omega', \theta_x)] \cdot I_{\text{PXR}}(\theta_x, \theta_y)\, d\theta_y\,. \tag{5}$$

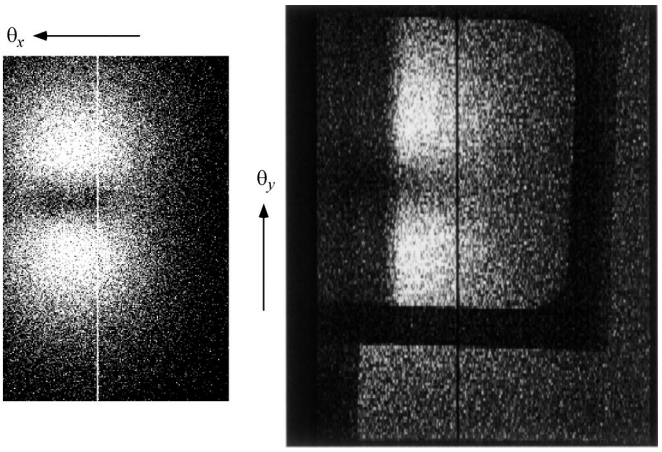

FIG. 2. (left) Two dimensional sum image of 100 exposures. The image shows the PXR angular distribution from the (022) plane of a silicon single crystal at a Bragg angle of 22.4°. The center of the dark area in the middle of the distribution coincides with the Bragg direction where the PXR intensity vanishes. The white line in the image is caused by dead CCD pixels. (right) Sum image of 250 exposures with a 6 μm thick nickel absorber foil ($E_k = 8332$ eV) in front of the CCD detector; see Fig. 1. The frame supporting absorber foil is visible as a dark shadow. Here the black line in the image is caused by dead CCD pixels.

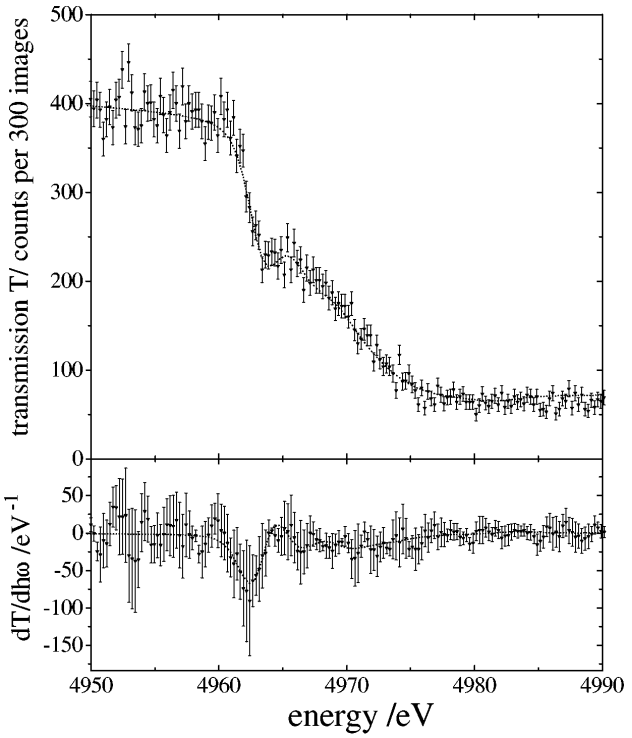

FIG. 3. Transmitted intensity $T(\hbar\omega)$ of PXR from the (111) plane of a silicon single crystal through a titanium foil at a Bragg angle of 23.2°. The lower panel shows the derivatives $T'(\hbar\omega)$ of the transmission. The dashed lines represent the best fit of Eq. (5) to the data.

This expression is a convolution ($\otimes$) of the transmission function of the absorber foil $T_{\mu a}(\hbar\omega') = \exp[-\mu(\hbar\omega')d]$ which takes into account the XANES structures and a Gaussian profile $g(\hbar\omega', \theta_x) = \exp\{-[\hbar\omega_B - \hbar\omega' + (\hbar\omega_B/\tan\theta_B)\theta_x]^2/(2\sigma_{\rm tot}^2)\}$ which describes the line shape of PXR and is itself a convolution of all the geometrical effects discussed above and including a possible intrinsic width. $I_{\rm PXR}(\theta_x, \theta_y)$ represents the calculated PXR intensity distribution [see Eq. (1) of Ref. [8]], and N is a normalization factor. The best fit as indicated by the dotted lines in Fig. 3 was obtained for a total width $\Delta\hbar\omega_{\rm tot} = \sqrt{8\ln 2}\,\sigma_{\rm tot} = (1.9 \pm 0.3)$ eV and (5.9 ± 0.7) eV (FWHM) for the PXR from the (111) plane of silicon at $\hbar\omega = 4966$ eV and (022) plane at $\hbar\omega = 8332$ eV, respectively.

The experimentally determined widths are somewhat larger than the calculated values of 1.2 and 3.6 eV which have been obtained taking the measured beam spot size of 75 ± 25 μm. In view of the relatively large uncertainty of the beam spot size it is not possible to assign the broadening to an effect of an intrinsic linewidth. Assuming that the beam spot size is 120 μm results according to Eq. (3) in linewidths of 1.9 and 5.8 eV in good agreement with the measured values. Therefore, upper limits of 1.2 and 3.5 eV (95% C.L.) can be estimated for the $\hbar\omega = 4966$ and 8332 eV, respectively.

A mosaicity of the crystal explaining the upper limit has to be as large as $9''$ (1σ) and is excluded. The natural linewidths from a perfect single crystal would amount to 20 and 2.5 meV, respectively. The geometrical contribution could be brought down to match these widths for the 4966 eV line by increasing the distance between Si crystal and detector from $L = 1$ to 10 m. In this way a width of 20 meV could be obtained which is a factor 33 narrower than the Darwin width of the Bragg reflex from the corresponding (111) plane. Extremely narrow linewidths should be observed in backward direction from a diamond single crystal. However, for this special geometry Eqs. (2), (3), and (4) do not apply, and a separate analysis is required.

This work is supported by the Deutsche Forschungsgemeinschaft DFG (SFB 201) and the Bundesministerium für Bildung und Forschung (06 MZ 566).

[1] V. Baryshevsky and I. Feranchuk, J. Phys. (Paris) **44**, 913 (1983).
[2] I. Feranchuk and A. Ivashin, J. Phys. (Paris) **46**, 1981 (1985).
[3] M. Ter-Mikaelian, *High-Energy Electromagnetic Processes in Condensed Media* (Wiley-Interscience, New York, London, Sydney, Toronto, 1972).
[4] H. Nitta, Phys. Lett. A **158**, 270 (1991).
[5] A. Caticha, Phys. Rev. B **45**, 9541 (1992).
[6] A. V. Shchagin, V. I. Pristupa, and N. A. Khizhnyak, Phys. Lett. A **148**, 485 (1990).
[7] J. Freudenberger *et al.*, Phys. Rev. Lett. **74**, 2487 (1995).
[8] K.-H. Brenzinger *et al.*, Z. Phys. A **358**, 107 (1997).
[9] J. Freudenberger *et al.*, Appl. Phys. Lett. **70**, 267 (1997).
[10] V. G. Baryshevsky and I. D. Feranchuk, Nucl. Instrum. Methods Phys. Res., Sect. A **228**, 490 (1985).
[11] R. B. Fiorito *et al.*, Nucl. Instrum. Methods Phys. Res., Sect. B **79**, 758 (1993).
[12] R. B. Fiorito *et al.*, Phys. Rev. E **51**, R2759 (1995).
[13] A. Caticha, Phys. Rev. A **40**, 4322 (1989).
[14] H. Backe *et al.*, Verh. Dtsch. Phys. Ges. (VI) **30**, 687 (1995).
[15] J. Rothe, Ph.D. thesis, Physikalisches Institut der Unviersität Bonn, 1996.
[16] S. Kraft, Ph.D. thesis, TU-Braunschweig, 1995.